IEEE Photonics Journal
An IEEE Photonics Society Publication

Open Access

Experimental Demonstration of a Multicorrugation-Pitch-Modulated (MCPM) DFB Semiconductor Laser Based on Reconstruction-Equivalent-Chirp Technology

Volume 7, Number 4, August 2015

Jilin Zheng
Yunshan Zhang
Yuechun Shi
Weichun Li
Bocang Qiu
Jun Lu
Tingting Zhang
Xiangfei Chen, Senior Member, IEEE

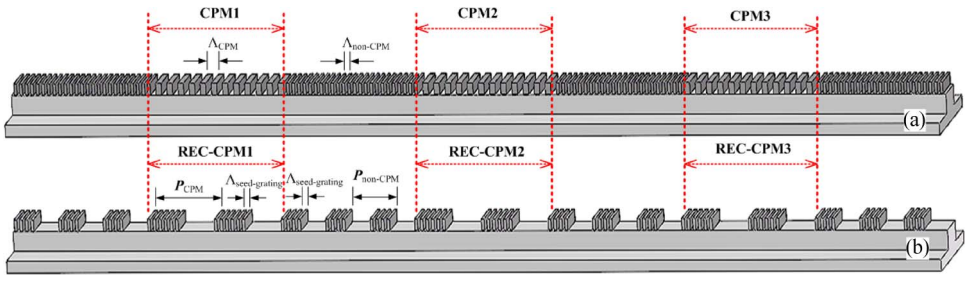

DOI: 10.1109/JPHOT.2015.2447456
1943-0655

IEEE photonics SOCIETY

IEEE

Experimental Demonstration of a Multicorrugation-Pitch-Modulated (MCPM) DFB Semiconductor Laser Based on Reconstruction-Equivalent-Chirp Technology

Jilin Zheng,[1,2] Yunshan Zhang,[1,3] Yuechun Shi,[1] Weichun Li,[1] Bocang Qiu,[4] Jun Lu,[1] Tingting Zhang,[1] and Xiangfei Chen,[1] *Senior Member, IEEE*

[1]Microwave-Photonics Technology Laboratory, National Laboratory of Microstructures, and School of Engineering and Applied Sciences, Nanjing University, Nanjing 210093, China
[2]Photonics Information Technology Laboratory, Institute of Communication Engineering, PLA University of Science and Technology, Nanjing 210007, China
[3]High-Tech Institute of Nanjing University, Suzhou 215123, China
[4]Suzhou Institute of Nano-Tech and Nano-Bionics, Chinese Academy of Sciences, Suzhou 215123, China

DOI: 10.1109/JPHOT.2015.2447456

Manuscript received May 31, 2015; revised June 10, 2015; accepted June 14, 2015. Date of publication June 19, 2015; date of current version July 1, 2015. This work was supported in part by the Natural Science Foundation of Jiangsu Province of China under Grant BK2012058, Grant BK20130585, and Grant BK20140414; by the National Natural Science Foundation of China under Grant 61306068 (Youth) and Grant 61435014; by the Applied Basic Research Project of Suzhou City under Grant SYG201309; by the China Postdoctoral Science Foundation under Grant 2013M531326; and by the National "863" Project under Grant 2015AA016902. Corresponding author: X. Chen (e-mail: chenxf@nju.edu.cn).

Abstract: A multicorrugation-pitch-modulated (MCPM) distributed-feedback semiconductor laser is experimentally demonstrated for the first time to achieve stable single longitudinal mode (SLM) performance. The MCPM structure was equivalently realized based on a sampled grating using reconstruction equivalent chirp (REC) technology. The proposed REC-MCPM structure can effectively flatten the optical intensity distribution along the laser cavity, leading to the strong suppression in spatial hole burning. In addition, the REC-MCPM grating structures can be readily fabricated using conventional holographic lithography combined with low-cost standard micrometer-level photolithography. A proof-of-principle study both in a simulation and an experiment is presented in this paper. The fabricated 400-μm-long REC-MCPM semiconductor laser shows very good SLM performance with SMSRs being more than 42 dB under test conditions of a large injection current range (up to 300 mA) and different ambient temperatures.

Index Terms: Distributed feedback (DFB) semiconductor laser, sampled grating, spatial-hole-burning.

1. Introduction

The distributed feedback (DFB) semiconductor laser is one of the most widely used optical sources for its exclusive performance and compact size. Usually, the grating structure of a DFB laser need to be well designed to achieve stable single-longitudinal-mode (SLM) operation. The most common structure is the quarter-wavelength-shifted (QWS) grating DFB lasers, which exhibit good SLM performance [1]. However, modal instabilities have often been observed

because of the spatial-hole-burning (SHB) effect at high injection current [2], [3], which degrades the performance of the lasers. To suppress the SHB effect, a variety of complicated grating structures have been proposed, such as corrugation-pitch-modulated (CPM) DFB lasers [4], distributed coupling coefficients (DCC) DFB lasers [5], multiple-phase-shift (MPS) DFB lasers [6], [7], and so on. Recently, multiple-CPM (MCPM) grating DFB lasers, which contain three CPM sections located along the longitudinal cavity, have been proposed and numerically investigated to further improve SLM performance [8]. The simulation results [8] indicate the MCPM DFB lasers have stronger ability to suppress the SHB effect and to maintain stable SLM operation compared with other approaches. However, in such an MCPM structure, the grating pitches in the CPM sections are different from that in non-CPM sections, and all the differences among multiple sections are required to be extremely small and accurate to produce desired distributed phase shifts. Thus it will be a rather challenging work to fabricate the complicated waveguide gratings with diverse grating pitches in the MCPM structure. In addition, experimental confirmation of MCPM DFB lasers is still highly required besides the prior simulation work. Most importantly, as well as other advanced performance DFB lasers with complicated structures, it is highly demanded that such reported three-CPM DFB lasers should be fabricated by commercial manufacturing methods with low cost, from the viewpoint of practicality.

In our previous work [9], we introduced the Reconstruction-Equivalent-Chirp (REC) technology [10]–[12] to equivalently realize the MCPM grating that can improve the SLM performance. The proposed REC-MCPM grating is an equivalent structure of the conventional MCPM grating that can suppress the SHB effect, the accuracy requirements for its realization however, is significantly relaxed. Such an REC-MCPM grating structure is formed based on a sampled Bragg grating with uniform seed grating pitch, and the sampling periods of the CPM regions are different from that of the non-CPM regions. Hence, the sampled Bragg grating can be defined by conventional holographic lithography combined with micrometer-level photolithography, since the seed grating is uniform, which offers the advantages of flexibility, high throughput and low-cost. Our previous work mainly focuses on the proposal of such a new concept however, further study in the static characteristics of REC-MCPM lasers and their SHB effect at high injection current is still highly required.

In this work, a proof-of-principle study both in simulation and experiment is presented. The simulation results showed the superiority of REC-MCPM lasers in reducing SHB effect and keeping SLM stability compared with the other two types of lasers, i.e., REC-CPM lasers and REC-3PS lasers, and the experimental results indeed showed good SLM performance can be maintained even under operation condition of high injection current. To the best of our knowledge, this is the first time of experimental demonstration of MCPM DFB lasers.

2. Principle and Simulation

2.1. REC-MCPM Grating Structure and Transmission Spectrum

The schematics of conventional real MCPM grating structure and the proposed REC-MCPM grating structure are shown in Fig. 1. In a real MCPM structure, the three CPM sections, where the grating pitch is longer than that of non-CPM sections, are introduced at the quarter, half and three quarters' positions of the cavity respectively. Since the grating pitches are usually on the order of 200 nm and the relative pitch difference between the CPM section and non-CPM section is as small as less than 3.4×10^{-3} (see [8]), complicated and expensive manufacturing methods of waveguide grating is required. While in REC-MCPM structure, conventional holographic lithography combined with standard micrometer-level photolithography can be employed to define sampling profiles, since the sampling periods are usually on the order of several micrometers, and the seed grating is uniform. By employing sampling functions with different sampling periods in the CPM sections, distributed phase shifts are thus obtained.

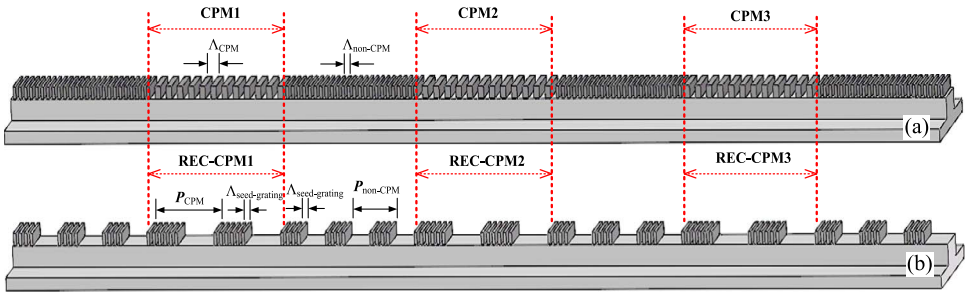

Fig. 1. Schematics of grating profiles. (a) Real MCPM. (b) REC-MCPM. Here, in a real MCPM structure, the grating pitch of CPM section (Λ_{CPM}) is longer than that of non-CPM section $(\Lambda_{non\text{-}CPM})$. The REC-MCPM grating is a structure of sampled Bragg grating, where the seed grating pitch $(\Lambda_{seed\text{-}grating})$ is uniform along the entire grating, but the sampling period in the CPM section (P_{CPM}) is longer than that in non-CPM section $(P_{non\text{-}CPM})$.

Based on the *Fourier* analysis, the refractive index modulation of a sampled Bragg grating can be expressed as

$$\Delta n(z) = \overline{\delta n}_{eff}(z) + \frac{1}{2}\sum_{m} \overline{\delta n}_{eff}(z) v(z) F_m \exp\left[-jm\phi(z) + j\frac{2\pi z}{\Lambda_m}\right] + c.c. \tag{1}$$

Here, $\overline{\delta n}_{eff}(z)$ is the average effective refractive index modulation, $v(z)$ is the fringe visibility that also acts as the apodization function, m is the order of the *Fourier* components, and F_m is the mth order *Fourier* coefficient. $\phi(z)$ is the chirped modulation realized by sampled grating. Λ_m is the grating pitch of mth order sub-grating, which can be expressed as

$$\Lambda_m = \frac{\Lambda_{\text{seed grating}} P}{m\Lambda_{\text{seed grating}} + P} \tag{2}$$

where $\Lambda_{seed\text{-}grating}$ is the seed grating pitch and P is the sampling period. Equation (2) shows Λ_m is jointly determined by P and $\Lambda_{seed\text{-}grating}$. From (2), one can see that it is possible to equivalently realize different grating with distinct grating pitch in the +1st order by choosing different sampling period P, even if seed grating pitch $\Lambda_{seed\text{-}grating}$ keeps constant. The Bragg wavelength of the 0th order sub-grating can be designed such that the wavelength position is located outside of the material gain region and the +1st order sub-grating is located within gain region for lasing.

To acquire an equivalent distributed phase shift Ψ, we should design the sampling period according to the following equation:

$$P_{CPM} = \frac{P_{non\text{-}CPM}}{1 - ((\psi P_{non\text{-}CPM})/(2\pi D_s))} \tag{3}$$

where $P_{non\text{-}CPM}$ is the sampling period out of CPM section, P_{CPM} is the sampling period within CPM section, and D_s is the length of the single CPM section. Properties of REC-MCPM structures can be similar to those of the conventional MCPM provided the parameters are carefully chosen.

To demonstrate that the proposed REC-MCPM structure has the same spectral characteristics as that for a regular MCPM grating structure, we calculate the transmission spectral responses for both structures based on the transmission matrix method (TMM) [13], [14]. Table 1 lists the simulation parameters for the REC three-CPM DFB laser. Here, we briefly explain the coupling coefficient of such an equivalent MCPM grating. Based on the *Fourier* analysis, the coupling coefficient of mth sub-grating κ_m in a sampled Bragg grating can be expressed as [15], [16]

$$\kappa_m = \kappa_0 \frac{\sin(\pi m\gamma)}{m\pi} \exp(-i\pi m\gamma) \tag{4}$$

TABLE 1
Parameters used in the simulation of REC-MCPM DFB lasers

Parameter	Value
Cavity length (L)	400 μm
Total length of CPM sections (D)	200 μm
Average effective refractive index (n_{eff})	3.2425
Pitch of the seed grating ($\Lambda_{seed\text{-}grating}$)	211.1 nm
Sampling period out of the CPM sections ($P_{non\text{-}CPM}$)	4.68 μm
Sampling period within the CPM sections (P_{CPM})	4.78 μm
Duty cycle of the equivalent MCPM grating (γ)	0.5
Index modulation of the equivalent MCPM grating (κ)	75 cm^{-1}
Linewidth enhancement factor (β)	1.5
Transparency carrier density (N_t)	1.2e18 cm^{-3}
Optical confinement factor (Γ)	0.3

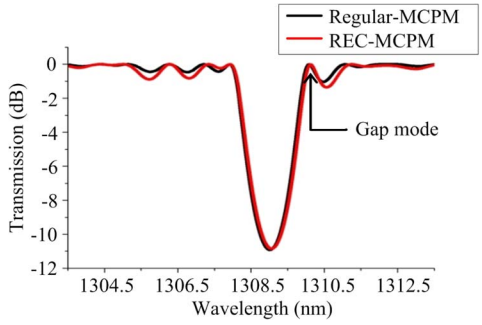

Fig. 2. Transmission spectra of MCPM and REC-MCPM gratings.

where κ_0 is the coupling coefficient of uniform seed grating, and γ is the duty cycle of the sampling structure. Hence, different γ can lead to different $\kappa_{\pm 1}$ in $\pm$1st sub-grating. In order to obtain the largest value of $\kappa_{\pm 1}$, $\gamma = 0.5$ is used in this work.

For the regular three-CPM structure, the cavity length L is 400 μm, the total length of CPM regions is 200 μm, the grating pitch of CPM regions is 202.1 nm, the grating pitch of non-CPM regions is 202.0 nm, and the average effective refractive index is 3.2425. It should be noted that the grating pitches of regular three-CPM structure are chosen different from that of REC three-CPM structure, which is carefully designed to compare their spectral characteristics in the same spectral range, because it is the +1st order sub-grating of REC three-CPM structure that is used for lasing while the 0th order sub-grating for regular three-CPM. The simulation results are plotted in Fig. 2. As can be seen, the REC three-CPM grating has the same transmission spectrum within the target band as that of the regular three-CPM grating. Most importantly, for the conventional three-CPM structure, the difference of grating pitches between CPM section and non-CPM section is 0.1 nm (202.1 nm minus 202.0 nm), while for REC three-CPM structure, the difference of sampling periods between CPM section and non-CPM section increases up to 0.1 μm (4.78 μm minus 4.68 μm). So, the accuracy requirements for the realization of REC-MCPM structure is significantly relaxed. It should be noted that the asymmetry of the gap mode indicates a tradeoff should be made between the side-mode suppression ratio (SMSR) and the reduction of SHB effect [17].

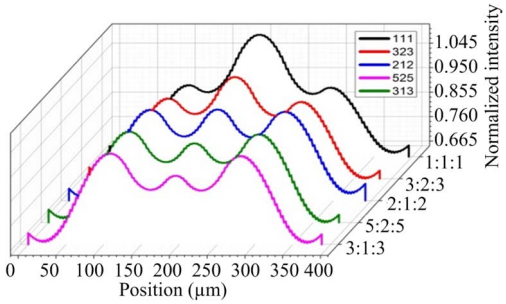

Fig. 3. Optical Intensity distribution of REC-MCPM DFB lasers with $D_1 : D_2 : D_3 = 1 : 1 : 1, 3 : 2 : 3, 2 : 1 : 2, 5 : 2 : 5, 3 : 1 : 3$.

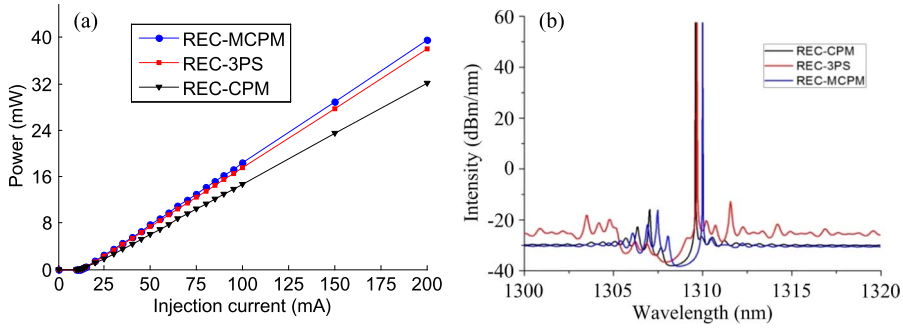

Fig. 4. (a) P-I curves of the REC-CPM DFB laser, the REC-3PS DFB laser, and the REC-MCPM DFB laser. (b) Spectra of the three types of DFB lasers.

2.2. Numerical Simulation of REC-MCPM DFB Semiconductor Lasers

The static characteristics of the DFB lasers are simulated using the TMM method [13], [14]. In the simulation of REC-MCPM DFB lasers, the total length of the CPM sections is fixed to be D, and the lengths of CPM1, CPM2 and CPM3 sections are D_1, D_2, and D_3 respectively $(D = D_1 + D_2 + D_3)$. When D_1, D_2, and D_3 change, the optical intensity distribution will also change. Here $D_1 = D_3 \neq D_2$. Normalized optical Intensity distribution of REC-MCPM DFB lasers with $D_1 : D_2 : D_3 = 1 : 1 : 1, 3 : 2 : 3, 2 : 1 : 2, 5 : 2 : 5, 3 : 1 : 3$ are numerically studied, which is shown in Fig. 3. In the following study, we choose the REC-MCPM DFB laser with $D_1 : D_2 : D_3 = 2 : 1 : 2$, because of its relatively flatter intensity distribution.

For comparison, a CPM DFB laser based on REC technology (REC-CPM) and a three phase shifts DFB laser based on REC technology (REC-3PS) are also analyzed. For the REC-CPM structure, the total cavity length is 400 μm, the CPM length is 200 μm and the distributed phase shift is π. For the REC-3PS structure, the total cavity length is also 400 μm, all the three phase shifts are $2\pi/3$, which are located in the quarter, half and three quarters' positions of the cavity respectively. Fig. 4(a) represents the power-injection current (P-I) performances of the three lasers at 1310-nm band. The threshold currents of the three types of lasers are almost identical, which is about 11 mA. The REC-MCPM DFB laser exhibits better performance in slope efficiency than the other two types of lasers, which is about 0.21 W/A. The simulated lasing spectra of the three lasers at the injection current of 60 mA are shown in Fig. 4(b) based on the model in [18], from which one can see the REC-MCPM DFB laser shows equally good SMSR performance to that of the other two types of lasers.

Fig. 5(a) shows the normalized optical intensity distribution of the three lasers being investigated. The results show that REC-MCPM DFB laser tends to have much flatter intensity distribution along the cavity than that for the other two types of lasers, which in turn will have stronger suppression to the SHB effect.

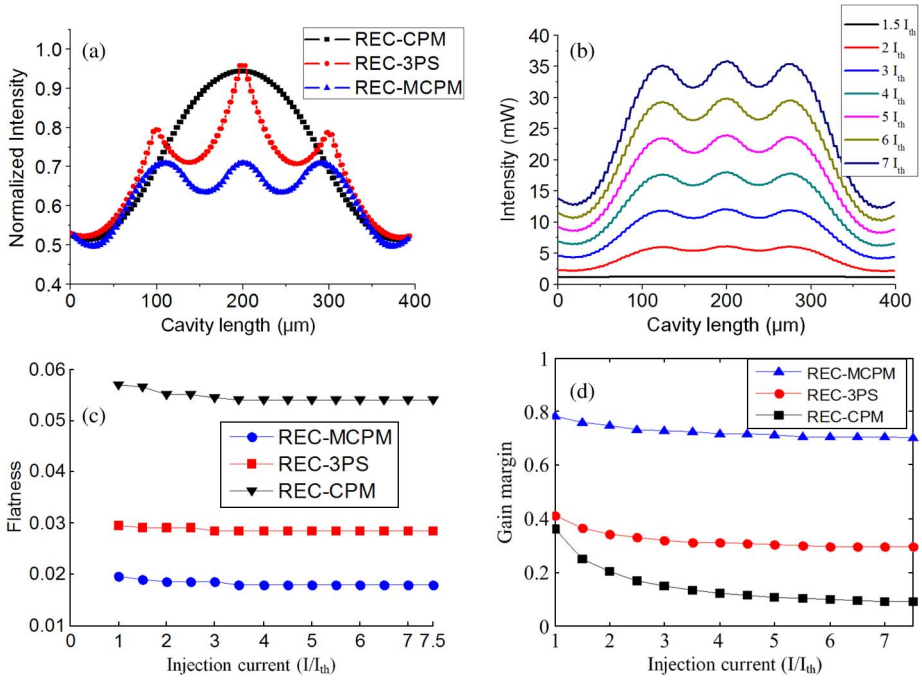

Fig. 5. (a) Normalized optical intensity distribution for the REC-CPM DFB laser, the REC-3PS DFB laser, and the REC-MCPM DFB laser. (b) Optical intensity distribution of the REC-MCPM DFB laser under different injection currents. (c) F-I curves for the three types of lasers. (d) Gain margins under different injection currents.

The optical intensity distribution of the REC-MCPM DFB laser under different injection currents is also simulated, which is shown in Fig. 5(b). Due to the stimulated emission, gradual increase of the optical intensity in the whole structure can be observed. However, good uniformity of the optical intensity distribution can be maintained with the increase of injection current.

From [19] and [20], the flatness factor can be expressed as

$$F = \frac{1}{L}\int_0^L \left(P(z) - \overline{P}\right)^2 dz. \tag{5}$$

$P(z)$ is the normalized optical intensity at the position of z along the cavity, and L is the length of the cavity. $\overline{P}$ denotes the average normalized optical intensity of the laser. From the definition in (5), one can see the more uniform the optical intensity distribution, the smaller the flatness factor, and the flatness factor becomes zero when the distribution is completely uniform. Fig. 5(c) shows the flatness factor versus injection current (F-I) performance of the three types of DFB lasers. As expected, the REC-MCPM DFB laser has the lowest value of flatness factor.

The effect of SHB on the laser performance with different injection current levels is also assessed. The gain margins under different injection currents are shown in Fig. 5(d). The gain margin is defined as the difference between the net gain of the main mode and that of the first side mode [21]. As can be seen, the REC-MCPM laser shows better mode selectivity compared with the other two types of lasers, which is an indication of stronger SLM stability under high injection current.

3. Experimental Results

The REC-MCPM DFB semiconductor laser was grown by a conventional two-stage lower-pressure metal-organic vapor phase epitaxy (MOVPE). The active region is composed of InGaAsP multiple-quantum-well (MQW). The uniform seeding grating was formed by conventional

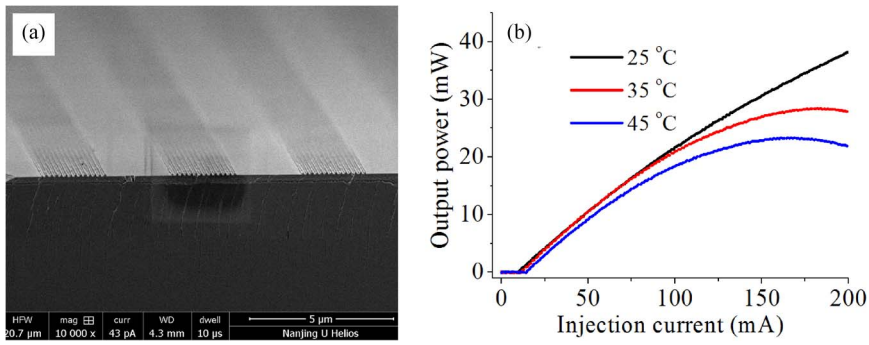

Fig. 6. (a) SEM image of the sampled gratings. (b) Measured P-I curves of the REC-MCPM DFB semiconductor laser at different ambient temperatures.

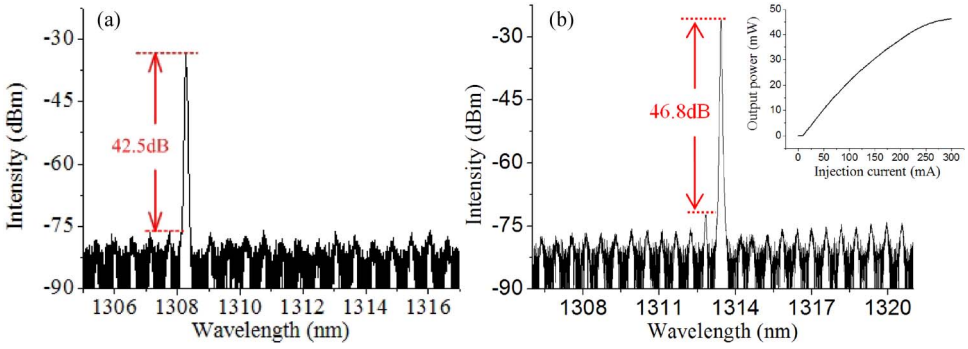

Fig. 7. Spectrum of REC-MCPM DFB laser under injection current of (a) 20 mA and (b) 300 mA. The inset is the P-I curve.

holographic exposure and the sampling profile was defined by micrometer-level photolithography, rendering the entire procedures for fabricating the REC-MCPM grating structure cost-effective since both the holographic exposure and micrometer-level photolithography offer mature fabrication and high throughput. A 2 μm ridge waveguide is used to guide light. Both the front facet and the rear facets were coated by anti-reflection (AR) coatings ($\sim$1%). The length of the laser is 400 μm, D is 200 μm, and $D_1 : D_2 : D_3 = 2 : 1 : 2$. The $P_{\text{non-CPM}}$ and P_{CPM} are 4.68 μm and 4.78 μm, respectively. The scanning electron microscope (SEM) image of part of the sampled grating is shown in Fig. 6(a). The laser was tested under CW operation and a thermoelectric cooler (TEC) was used to control the temperature. The P-I characteristics of the laser at different ambient temperatures are shown in Fig. 6(b). The threshold current of the laser is 11 mA at 25 °C and the slope efficiency is about 0.2 W/A. When the temperature rises to 45 °C, the threshold current increases to 15 mA and the slope efficiency decreases to about 0.12 W/A.

The SLM performance of the fabricated REC-MCPM semiconductor laser under different injection current levels was evaluated. Fig. 7(a) shows the spectra of the REC-MCPM laser under the injection current of 20 mA at room temperature (25 °C), whose SMSR reaches 42.5 dB. It should be noted that periodic side-modes can been observed, which can be enhanced by increasing the injection current to 300 mA [shown in Fig. 7(b)]. Such a strongly periodic modal structure is attributed to the Fabry-Perot mode that is induced by the imperfection of AR coatings of both facets ($\sim$1%). This judgment is also confirmed by the fact that the mode spacing, which is about 0.6 nm, is in good agreement with the 400 μm-long Fabry-Perot cavity length. From Fig. 7(b), however, we can find the laser still exhibits good SLM operation with SMSR being about 46.8 dB. The spectra of the REC-MCPM laser under the injection current ranging from 20 mA to 300 mA at room temperature are also shown in Fig. 8(a), from which one can see that

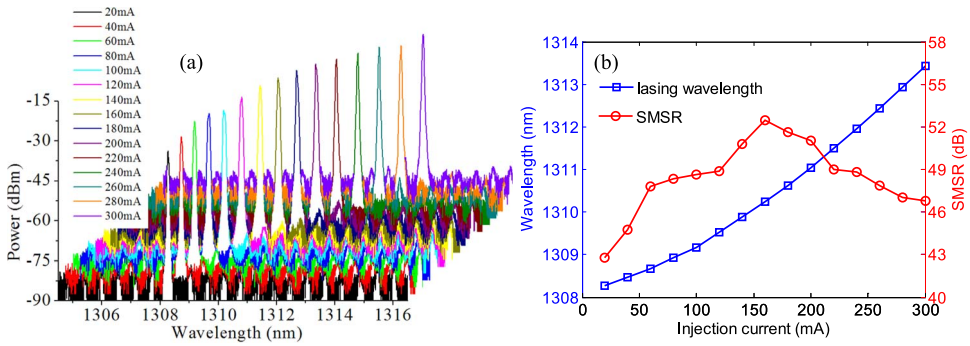

Fig. 8. (a) Spectra of the REC-MCPM laser under different injection current levels. (b) Measured lasing wavelengths and SMSRs of the REC-MCPM DFB laser under different injection currents.

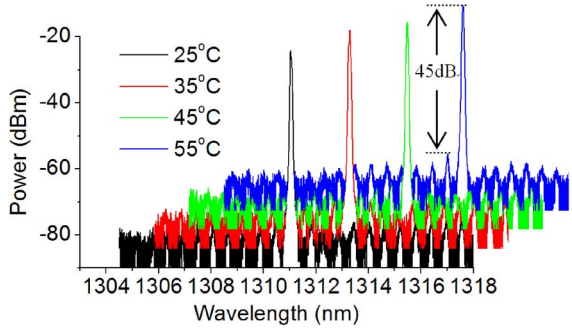

Fig. 9. Spectra of REC-MCPM DFB laser under 200 mA at different ambient temperatures.

very stable SLM operation is maintained. From the measured results, the lasing wavelengths and SMSRs under different injection current can be extracted and are plotted in Fig. 8(b). As can be seen, the lasing wavelengths shift to longer wavelengths when the injection current increases. The dominating mechanism is attributed to the thermal effect, which is similar to what has been observed in [15]. Although the SMSRs begin to decline when the injection current is larger than 150 mA, good SMSR performance ($>$ 42 dB) is obtained for entire current range from 20 mA to 300 mA. Such a good SLM performance under high injection current is directly associated to the reduction in the SHB effect.

The lasing characteristics at different ambient temperatures were also tested. Fig. 9 shows the spectra of the REC-MCPM laser under 200 mA at ambient temperatures of 25 °C, 35 °C, 45 °C, and 55 °C respectively. It can be seen stable SLM operation with SMSRs $>$ 45 dB is maintained.

4. Conclusion

An MCPM grating DFB semiconductor laser has been experimentally demonstrated for the first time based on the REC technology. The REC-MCPM grating structure has the same spectral characteristics as the for a conventional MCPM grating, its fabrication process however, is significantly simplified, because conventional holographic lithography combined with μm-level photolithography can be employed. The simulation results reveal the advantages of the REC-MCPM laser in suppressing the SHB effect over the lasers using the other two methods, i.e., CPM and 3PS. The experimental results has confirmed that such an REC-MCPM semiconductor laser can indeed produce superior SLM performance with large injection current range due to the reduction in SHB effect. Therefore, the proposed method offers a practical and low-cost method for the realization of DFB semiconductor lasers with highly stable SLM performance.

Such a method can also find its application in realizing DFB lasers with extremely narrow linewidth by dramatically extending the cavity length where the SHB effect is a matter of severe concern. In the future, realizing narrow linewidth lasers based on optimized REC-MCPM structures would be another significant work.

References

[1] S. Akiba, M. Usami, and K. Utaka, "1.5-μm $\lambda/4$-shifted InGaAsP/InP DFB lasers," *J. Lightw. Technol.*, vol. LT-5, no. 11, pp. 1564–1573, Nov. 1987.

[2] P. Correc, "Stability of phase-shifted DFB lasers against hole burning," *IEEE J. Quantum Electron.*, vol. 30, no. 11, pp. 2467–2476, Nov. 1994.

[3] J. E. A. Whiteaway, G. H. B. Thompson, A. J. Collar, and C. J. Armistead, "The design assessment of $\lambda/4$ phase shifted DFB laser structures," *IEEE J. Quantum Electron.*, vol. 25, no. 6, pp. 1261–1279, Jun. 1989.

[4] M. Okai, N. Chinone, H. Taira, and T. Harada, "Corrugation-pitch-modulated phase-shifted DFB laser," *IEEE Photon. Technol. Lett.*, vol. 1, no. 8, pp. 200–201, Aug. 1989.

[5] B. S. K. Lo and H. Ghafouri-Shiraz, "Spectral characteristics of distributed feedback laser diodes with distributed coupling coefficient," *J. Lightw. Technol.*, vol. 13, no. 2, pp. 200–212, Feb. 1995.

[6] G. P. Agrawal, J. E. Geusic, and P. J. Anthony, "Distributed feedback lasers with multiple phase-shift regions," *Appl. Phys. Lett.*, vol. 53, no. 3, pp. 178–179, Jul. 1988.

[7] L. Lu *et al.*, "Experimental demonstration of the three-phase-shifted DFB semiconductor laser with buried heterostructure using common holographic exposure," *Sci. China Tech. Sci.*, vol. 57, no. 11, pp. 2231–2235, Nov. 2014.

[8] Q. Zuo, J. Zhao, Z. Wang, X. Chen, and W. Liu, "High performance asymmetric three corrugation-pitch-modulated DFB lasers suitable for stable single longitudinal mode operation," *Opt. Photon. J.*, vol. 3, no. 2, pp. 57–60, Jun. 2013.

[9] W. Li, J. Zheng, J. Zheng, and X. Chen, "Numerical study of a DFB semiconductor laser with Multi-Corrugation-Pitch-Modulated (MCPM) structure based on Reconstruction-Equivalent-Chirp (REC) technology," presented at the Asia Commun. Photon. Conf., Nov. 2013, AF2F.28.

[10] Y. Dai and X. Chen, "DFB semiconductor lasers based on reconstruction-equivalent-chirp technology," *Opt. Exp.*, vol. 15, no. 5, pp. 2348–2353, Mar. 2007.

[11] J. Li *et al.*, "Experimental demonstration of distributed feedback lasers based on reconstruction-equivalent-chirp technology," *Opt. Exp.*, vol. 17, no. 7, pp. 5240–5245, Mar. 2009.

[12] L. Lu *et al.*, "Experimental demonstration of $\lambda/8$ DFB semiconductor laser array for 1.3 μm CWDM system," *Sci. China Tech. Sci.*, vol. 57, no. 9, pp. 1769–1772, Sep. 2014.

[13] T. Erdogan, "Fiber grating spectra," *J. Lightw. Technol.*, vol. 15, no. 8, pp. 1277–1294, Aug. 1997.

[14] S. K. B. Lo and H. Ghafouri-Shiraz, "A method to determine the above-threshold stability of distributed feedback semiconductor laser diodes," *J. Lightw. Technol.*, vol. 13, no. 4, pp. 563–568, Apr. 1995.

[15] S. Li *et al.*, "Experimental demonstration of DFB semiconductor lasers with varying longitudinal parameters," *Opt. Exp.*, vol. 22, no. 4, pp. 4059–4064, Feb. 2014.

[16] V. Veerasubramanian *et al.*, "Design and demonstration of apodized comb filters on SOI," *IEEE Photon. J.*, vol. 4, no. 4, pp. 1133–1139, Aug. 2012.

[17] Y. Dai and J. Yao, "Numerical study of a DFB semiconductor laser and laser array with chirped structure based on the equivalent chirp technology," *IEEE J. Quantum Electron.*, vol. 44, no. 10, pp. 938–945, Oct. 2008.

[18] W. Fang, A. Hsu, S. L. Chuang, T. Tanbun-Ek, and A. M. Sergent, "Measurement and modeling of distributed feedback lasers with spatial hole burning," *IEEE J. Sel. Top. Quantum Electron.*, vol. 3, no. 2, pp. 547–554, Apr. 1997.

[19] T. Kimura and A. Sugimura, "Coupled phase-shift distributed-feedback semiconductor lasers for Narrow linewidth operation," *IEEE J. Quantum Electron.*, vol. 25, no. 4, pp. 678–683, Apr. 1989.

[20] S. Yuechun, T. Xinghua, L. Simin, and Z. Yating, "Numerical study of three phase shifts and dual corrugation pitch modulated (CPM) DFB semiconductor lasers based on reconstruction equivalent chirp technology," *Chin. Sci. Bull.*, vol. 55, no. 19, pp. 1944–1950, Jul. 2010.

[21] T. Fessant, "Threshold and above-threshold analysis of corrugation-pitch-modulated DFB lasers with inhomogeneous coupling coefficient," *Proc. Inst. Elect. Eng.—Optoelectron.*, vol. 144, no. 6, pp. 365–376, Dec. 1997.